Lithium Hydrazinidoborane Ammoniate LiN2H3BH3×0.25NH3, a Derivative of Hydrazine Borane

Salem Ould-Amara, Dominique Granier, Rodica Chiriac, François Toche, Pascal G. Yot, Umit B. Demirci

materials

MDPI

Article

Lithium Hydrazinidoborane Ammoniate $LiN_2H_3BH_3 \cdot 0.25NH_3$, a Derivative of Hydrazine Borane

Salem Ould-Amara [1], Dominique Granier [2], Rodica Chiriac [3], François Toche [3], Pascal G. Yot [2] and Umit B. Demirci [1,*]

1 IEM (Institut Europeen des Membranes), UMR5635 (CNRS, ENSCM, UM), Universite de Montpellier, Place Eugene Bataillon, CC047, F-34095 Montpellier, France; salem.ould-amara@iemm.univ-montp2.fr
2 ICGM (Institut Charles Gerhardt Montpellier), UMR 5253 (CNRS UM ENSCM), Université de Montpellier, CC 15005, Place Eugène Bataillon, F-34095 Montpellier cedex 05, France; dominique.granier@umontpellier.com (D.G.); pascal.yot@umontpellier.fr (P.G.Y.)
3 Univ Lyon, Université Claude Bernard Lyon 1, Laboratoire des Multimatériaux et Interfaces UMR CNRS 5615, LMI, F-69622 Villeurbanne, France; rodica.chiriac@univ-lyon1.fr (R.C.); francois.toche@univ-lyon1.fr (F.T.)
* Correspondence: umit.demirci@umontpellier.fr; Tel.: +33-4-6714-9160

Received: 14 June 2017; Accepted: 29 June 2017; Published: 5 July 2017

Abstract: Boron- and nitrogen-based materials have shown to be attractive for solid-state chemical hydrogen storage owing to gravimetric hydrogen densities higher than 10 wt% H. Herein, we report a new derivative of hydrazine borane $N_2H_4BH_3$, namely lithium hydrazinidoborane ammoniate $LiN_2H_3BH_3 \cdot 0.25NH_3$. It is easily obtained in ambient conditions by ball-milling $N_2H_4BH_3$ and lithium amide $LiNH_2$ taken in equimolar amounts. Both compounds react without loss of any H atoms. The molecular and crystallographic structures of our new compound have been confirmed by NMR/FTIR spectroscopy and powder X-ray diffraction. The complexation of the entity $LiN_2H_3BH_3$ by some NH_3 has been also established by thermogravimetric and calorimetric analyses. In our conditions, $LiN_2H_3BH_3 \cdot 0.25NH_3$ has been shown to be able to release H_2 at temperatures lower than the parent $N_2H_4BH_3$ or the counterpart $LiN_2H_3BH_3$. It also liberates non-negligible amounts of NH_3 at temperatures lower than 100 °C. This is actually quite detrimental for chemical H storage, but alternatively $LiN_2H_3BH_3 \cdot 0.25NH_3$ might be seen as a potential NH_3 carrier.

Keywords: ammonia carrier; ammoniate; borane; hydrazine borane; hydrazinidoborane; chemical hydrogen storage

1. Introduction

Hydrogen storage is one of the major obstacles restricting the development of an "economy of hydrogen energy". Within the past decade, many studies have been done to find new solutions, and particular attention has been paid to chemical H storage [1], and interestingly there has been new interest in old molecules and materials [2]. An example of this is hydrazine borane $N_2H_4BH_3$. It was discovered in the 1960s and the first applied study presented it as an energetic material [3]. It was then barely investigated until recent years. In 2009, $N_2H_4BH_3$ was re-discovered owing to its high gravimetric hydrogen density of 15.4 wt%. However, it was considered as being unsuitable for solid-state chemical H storage because of hazardous dehydrogenation properties [4]. Indeed, when heated it releases large amounts of hydrazine N_2H_4 together with H_2, and generates a shock-sensitive solid residue above 300 °C [5]. It is worth mentioning that hydrogen storage via hydrazine borane and any other B–N–H compounds (e.g., ammonia borane NH_3BH_3) is irreversible. Upon thermolytic dehydrogenation, they transform into a polymeric residue of complex composition

and they cannot be hydrogenated directly under H_2 pressure. The only way to regenerate the starting materials is chemical recycling [1,2].

Yet, $N_2H_4BH_3$ is still of interest in the field because it can be modified by reaction with an alkali hydride MH (M^+ = Li^+, Na^+, K^+) resulting in the formation of an alkali hydrazinidoborane derivative, $MN_2H_3BH_3$ [6]:

$$N_2H_4BH_3\ (s) + MH\ (s) \rightarrow MN_2H_3BH_3\ (s) + H_2\ (g) \quad (1)$$

Lithium hydrazinidoborane $LiN_2H_3BH_3$ is synthesized by ball-milling and depending on the milling conditions, two polymorphs form. The α phase (monoclinic, s.g. (space group) $P2_1/c$), already reported [7], is the high-temperature phase. It can be synthesized directly [7]. Otherwise it can be formed from the β phase (orthorhombic, s.g. *Pbca*) at about 95 °C [8]. The latter phase is the low-temperature phase. Lithium hydrazinidoborane is thermally less stable than the parent $N_2H_4BH_3$ as a result of the substitution of one $H^{\delta+}$ of the N_2H_4 moiety by Li^+ and of the subsequent lengthening and concomitant weakening of the $H^{\delta+}\cdots H^{\delta-}$ interactions (which refer to the so-called dihydrogen bonding). For example, the β phase is able to dehydrogenate from 40 °C and release 7.8 wt% of almost pure H_2 up to 144 °C. Lithium hydrazinidoborane is thus more suitable for solid-state chemical H storage than the parent $N_2H_4BH_3$. This is also the case for the sodium derivative $NaN_2H_3BH_3$ [9]. It starts to liberate H_2 below 60 °C, and over the range 60–100 °C it loses 6 wt% of almost pure H_2. The interesting feature with $NaN_2H_3BH_3$ is that synthesis by ball-milling has to be performed below −30 °C because of the high reactivity of sodium hydride NaH with $N_2H_4BH_3$. A reaction enthalpy of −27,756.7 J mol^{-1} was determined by Calvet calorimetry at 25 °C [10]. The reaction is highly exothermic, especially when compared to the enthalpy of the reaction between LiH and $N_2H_4BH_3$ at the same temperature (−62.8 J mol^{-1}). In fact, the bigger the alkali cation is, the more exothermic the reactivity of the alkali hydride. The enthalpy of reaction of KH with $N_2H_4BH_3$ was measured as being −70,247.2 J mol^{-1}. Accordingly, the safest way to get potassium hydrazinidoborane $KN_2H_3BH_3$ is by wet synthesis (i.e., suspension in tetrahydrofuran) in an autoclave reactor [11]. All of these alkali hydrazinidoboranes have shown better and safer dehydrogenation properties than the parent hydrazine borane. To our knowledge, there is no other derivative of $N_2H_4BH_3$. Attempts in synthesizing the hydrazinidoboranes of magnesium, calcium, and aluminum $M(N_2H_3BH_3)_n$ (M^{n+} = Mg^{2+}, Ca^{2+}, Al^{3+}) by ball-milling have failed. Composites MH_n-$N_2H_4BH_3$ have been found to form where the hydrides act as destabilizers of the borane [10].

The substitution of one $H^{\delta+}$ of the N_2H_4 moiety of $N_2H_4BH_3$ by M^+ negatively affects the gravimetric hydrogen density of the as-formed material because of the loss of 1 equivalent of H_2. For instance, the gravimetric hydrogen density drops from 15.4 wt% for $N_2H_4BH_3$ to 11.7, 8.9, and 7.2 wt% for $LiN_2H_3BH_3$, $NaN_2H_3BH_3$, and $KN_2H_3BH_3$, respectively. The decrease might be compensated by using an amide MNH_2 instead of a hydride MH, only if the NH_2 group of the amide interacts by trapping one $H^{\delta+}$ of the N_2H_4 moiety of hydrazine borane. Consequently, the formation of a new compound may be expected with a formula resembling $MN_2H_3BH_3{\cdot}xNH_3$. Such an approach has shown to be successful for synthesizing metal amidoborane ammoniates like $Mg(NH_2BH_3){\cdot}NH_3$ and $Ca(NH_2BH_3){\cdot}NH_3$ where all of the hydrogen atoms of the precursors were kept in the final material [12,13]. We therefore explored the possibility of synthesizing novel derivatives of $N_2H_4BH_3$. Lithium amide $LiNH_2$ was selected owing to the lightness of Li^+. Another reason for this choice is that LiH is less reactive than NaH or KH, and thus is safer. Similar behavior was expected for $LiNH_2$. Then, by ball-milling $N_2H_4BH_3$ and $LiNH_2$, the formation of lithium hydrazinidoborane ammoniate $LiN_2H_3BH_3{\cdot}xNH_3$ was expected; it has a higher gravimetric hydrogen density (13.2 wt% for x = 1; 12.1 for x = 0.25) than $LiN_2H_3BH_3$ (11.6 wt%). This is discussed hereafter.

2. Results

2.1. Molecular Structure

Ball-milling of $LiNH_2$ and $N_2H_4BH_3$ in our conditions resulted in the formation of a pasty solid. More details are given in the section dedicated to the experimental conditions. The pasty aspect is otherwise discussed in the discussion section. Hereafter, the precursors $N_2H_4BH_3$ and $LiNH_2$ will be denoted **1** and **2** respectively, while the ball-milling product will be identified as **3**.

The ^{11}B MAS NMR spectra of **1** and **3** are shown in Figure 1. With the former (i.e., $N_2H_4BH_3$), the signal is typical of a quadrupolar coupling due to anisotropy around the boron atom because of strong intermolecular $H^{\delta+}\cdots H^{\delta-}$ interactions. In contrast, the new compound **3** shows a resonance of high intensity at δ −19.6 ppm; the signal is otherwise broad. Such features are indicative of isotropy around the boron atom of the NBH_3 environment, change of the environment of the N–H bonds, and lengthening of the intermolecular $H^{\delta+}\cdots H^{\delta-}$ interactions. Similar observations were reported for $LiN_2H_3BH_3$ as well as for $NaN_2H_3BH_3$ [6–9]. There are also two other signals. The first one is centered at δ −41.3 ppm. It is typical of a BH_4 environment [14]. The second one is centered at δ −6.7 ppm. It may be ascribed to N_2BH_2 and N_3BH environments [15]. The presence of such N_2BH_2 and N_3BH environments might indicate some decomposition of the starting borane, but the concomitant apparition of the BH_4 environment does not support such an assumption. In the open literature dedicated to B–N–H compounds, the presence of both signals is generally ascribed to the formation of an ionic dimer [16]: for example, with ammonia borane NH_3BH_3, a similar ^{11}B MAS NMR spectrum can be collected when part of the borane transforms to the ionic dimer diammoniate of diborane of formula $[NH_3BH_2NH_3^+][BH_4^-]$. We therefore believe that in our conditions a little part of $N_2H_4BH_3$ dimerized into an ionic intermediate of formula $[N_2H_4BH_2N_2H_4^+][BH_4^-]$ (dihydrazinoboronium borohydride or dihydrazinate of diborane):

$$2N_2H_4BH_3\ (s) \rightarrow [N_2H_4BH_2N_2H_4^+][BH_4^-]\ (s) \quad (2)$$

Such a compound shows both of the N_2BH_2 and BH_4 environments, while the BH_3 environment comes from the new solid **3**.

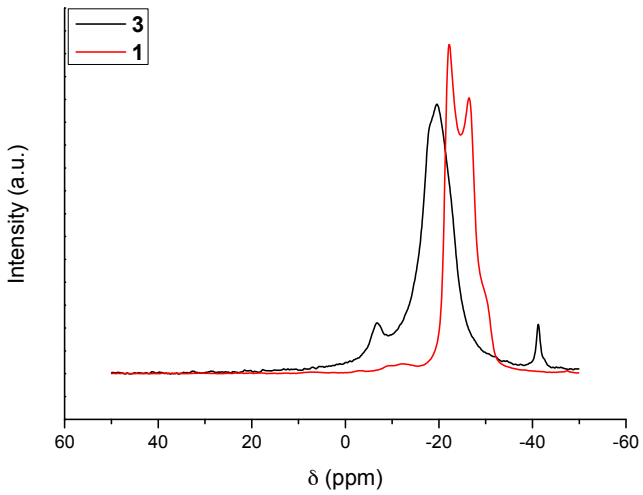

Figure 1. ^{11}B MAS NMR spectra of **3**. For comparison the spectrum of $N_2H_4BH_3$ (**1**) is shown.

The FTIR spectrum of **3** (Figure 2) is different from that of **1**. It displays a less complex fingerprint in the N–H stretching region (3450–2950 cm^{-1}) and broadened N–H bending bands (1700–1300 cm^{-1}), thereby suggesting that the intermolecular $H^{\delta+}\cdots H^{\delta-}$ interactions are less important and that the $H^{\delta+}\cdots H^{\delta-}$ network is weaker. There are more bands in the B–H stretching region

(2600–1800 cm^{-1}) owing to interactions of Li^+ and N of **2** with $H^{\delta-}$ of BH_3 groups. The two small bands at 1913 and 2017 cm^{-1} observed on the spectrum of $N_2H_4BH_3$ are indicative of strong $H^{\delta+}\cdots H^{\delta-}$ interactions [5]. They cannot be seen for **3**, confirming a weakened $H^{\delta+}\cdots H^{\delta-}$ network. It may be reasonably concluded that **2** has induced electronic modification in **1**. In fact, the FTIR spectrum of **3** resembles that of $LiN_2H_4BH_3$ reported elsewhere and similar conclusions were made for this derivative [8]. The N–H stretching vibration at 3375 cm^{-1} is in the range of the degenerate stretching N–H mode of ammonia, thereby suggesting weakly bound NH_3 molecules [17].

The aforementioned spectroscopy results are indicative of the formation of a compound with the speculated molecular formula $LiN_2H_3BH_3{\cdot}xNH_3$ (lithium hydrazinidoborane ammoniate).

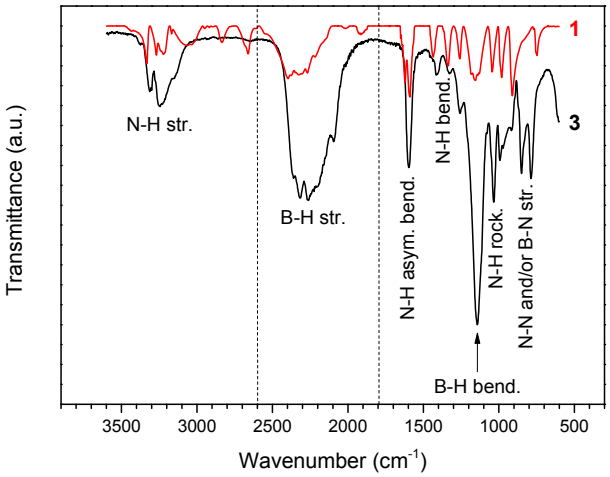

Figure 2. FTIR spectrum of **3** and, for comparison, that of **1** ($N_2H_4BH_3$). The different vibrational modes are indicated.

2.2. Crystallography

The powder XRD pattern recorded for **3** is shown in Figure 3. It was compared to the patterns of the reactants **1** [3,7,18] and **2** [19]. The presence of a new crystalline phase was confirmed, though some residual diffraction peaks coming from **2** have been also detected.

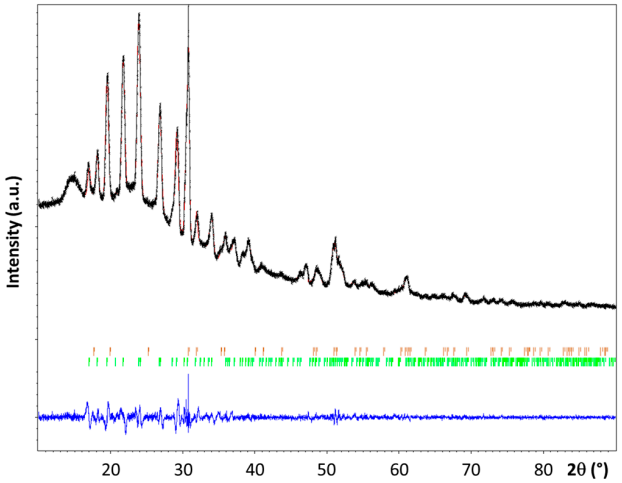

Figure 3. Observed (in black) and calculated (in red) powder X-ray diffraction profiles for the Rietveld refinement of the $LiN_2H_3BH_3{\cdot}xNH_3$ phase. The bottom curve (in blue) is the difference plot on the same scale intensity and the tick marks (in green for $LiN_2H_3BH_3{\cdot}xNH_3$ and in orange for $LiNH_2$) are the calculated angles for the Bragg peaks in 2θ (λ = 1.5418 Å).

The diffraction peaks of **3** have been successfully indexed as a single phase using DICVOL06 [20] after removing the peaks supposed to be overlapped with the $LiNH_2$ diffraction lines. The new phase **3** crystallizes in the monoclinic system, with a space group $P2_1/n$ (No. 14) and Z = 4; the unit cell parameters a = 7.649(1) Å, b = 7.502(1) Å, c = 5.973(1) Å, and β = 97.81(1)° were found. The unit cell volume (~340 $Å^3$) is larger than the one reported for α–$LiN_2H_3BH_3$ (328 $Å^3$) [7]. The structure factor of **3** and that of the α [7] and β [8] phases of $LiN_2H_3BH_3$ were compared; they present strong differences. This is indicative of the formation of a new phase. The position of the Li element in the unit cell was located by Direct Methods using EXPO2014 [21]. The crystal structure was then successfully refined by the Rietveld method (Figure 3) using the Jana 2006 program [22]. The structure parameters that were obtained are presented in Tables 1 and 2. For the refinement the lengths of the N–N and N–B bonds and the N–N–B angle were fixed to 1.50 Å, 1.58 Å, and 113.8° respectively. The refinement was carried out while taking into account the presence of **2**. As a result, the relative weight amounts of **3** ($LiN_2H_3BH_3 \cdot xNH_3$) and **2** ($LiNH_2$) were found to be close to be 95.4 and 4.6 wt%, respectively. Nevertheless, the refinement of the position of the *x* molecule of NH_3 into the crystalline network has not been possible. Hence, considering the difference of volume (14 $Å^3$) between the cell volume of **3** and that of α–$LiN_2H_3BH_3$, it can be assumed the presence of one non-H atom per unit cell. This atom is proposed to be N of NH_3, suggesting then the molecular formula $LiN_2H_3BH_3 \cdot 0.25NH_3$ for **3**.

Table 1. Space group (s.g.), unit cell parameters, goodness of fit, and R-values for the refined structures for **3** ($LiN_2H_3BH_3 \cdot xNH_3$) and **2** ($LiNH_2$) at room temperature.

	$LiN_2H_3BH_3 \cdot xNH_3$	**$LiNH_2$**
s.g.	$P2_1/n$ (N° 14)	$I\bar{4}$ (N° 82)
Z	4	8
a (Å)	7.6498(18)	5.1158(11)
b (Å)	7.482(3)	5.1158(11)
c (Å)	5.968(17)	10.103(3)
β (°)	97.803(12)	-
V ($Å^3$)	338.91(17)	264.41(12)
R.P.A. (wt%) [1]	95.4(5)%	4.6(6)%
GoF	2.94	2.94
Rp	3.66	3.66
wRp	486	4.86
R(obs)/R(all)	13.85/15.47	11.17/12.49
wR(obs)/wR(all)	11.66/11.77	11.92/12.00

[1] Relative phase amounts in weight.

Table 2. Experimental structural parameters of **3** ($LiN_2H_3BH_3 \cdot xNH_3$) and **2** ($LiNH_2$) at room temperature. The atomic positions for $LiNH_2$ were kept fixed during the refinement [19].

Sample	**Atom**	**Site**	**Occupancy**	**x**	**y**	**z**	**U_{iso} ($Å^2$)**
3	Li1_1	4e	1	0.4025(11)	0.4401(9)	0.767(2)	0.0229(1)
	B2_1	4e	1	0.7210(11)	0.3147(17)	0.5489(13)	0.0213(1)
	N3_1	4e	1	0.6451(11)	0.2980(11)	0.7827(11)	0.0202(1)
	N4_1	4e	1	0.6373(18)	0.1096(14)	0.867(3)	0.0202(1)
2	Li1_2	2a	1	0.00000	0.500000	0.25000	0.0177(1)
	Li2_2	2d	1	0.00000	0.00000	0.00000	0.0177(1)
	Li3_2	4e	1	0,00000	0.00000	0.25300	0.0177(1)
	N4_2	8g	1	0.23400	0.25400	0.13700	0.0065(1)

2.3. Thermal Analyses and Evolving Gas Analyses

Under heating at 5 °C min^{-1}, **3** is stable up to 75 °C (Figure 4). Then, it decomposes according to a complex pathway. The DSC curve is characterized by two major (maximum at 119.4 and 180.2 °C)

and two minor exothermic events (107.4 and 145.5 °C). This is consistent with the occurrence of several weight losses observed by TGA. Over 75 °C, **3** starts to liberate NH_3, which is characterized by the first exothermic event (0.9 kJ mol^{-1}) peaking at 107.4 °C. This is consistent with the molecular structure of an adduct like $LiN_2H_3BH_3 \cdot xNH_3$. The first major weight loss (8.3 wt%) that occurs over the temperature range 75–145 °C is associated with the second exothermic event (11.5 kJ mol^{-1}) peaking at 119.4 °C. It is mainly due to the dehydrogenation of **3**. There is then an exothermic signal of low heat (0.15 kJ mol^{-1}). It is followed by the second major decomposition (12.9 wt% and 50.5 kJ mol^{-1}) that takes place over the temperature range 145–300 °C. At 300 °C, the overall weight loss is 21.2 wt% and it cannot be rationalized with the loss of H_2 only (maximum of 13.2 wt% H in **3** if $x = 1$; 12.1 wt% H if $x = 0.25$). The weight proportion of NH_3 in the adduct $LiN_2H_3BH_3 \cdot xNH_3$ is theoretically of 24.7 wt% NH_3 if $x = 1$, and 7.6 wt% NH_3 if $x = 0.25$. Hence, **3** releases H_2 and significant amounts of NH_3.

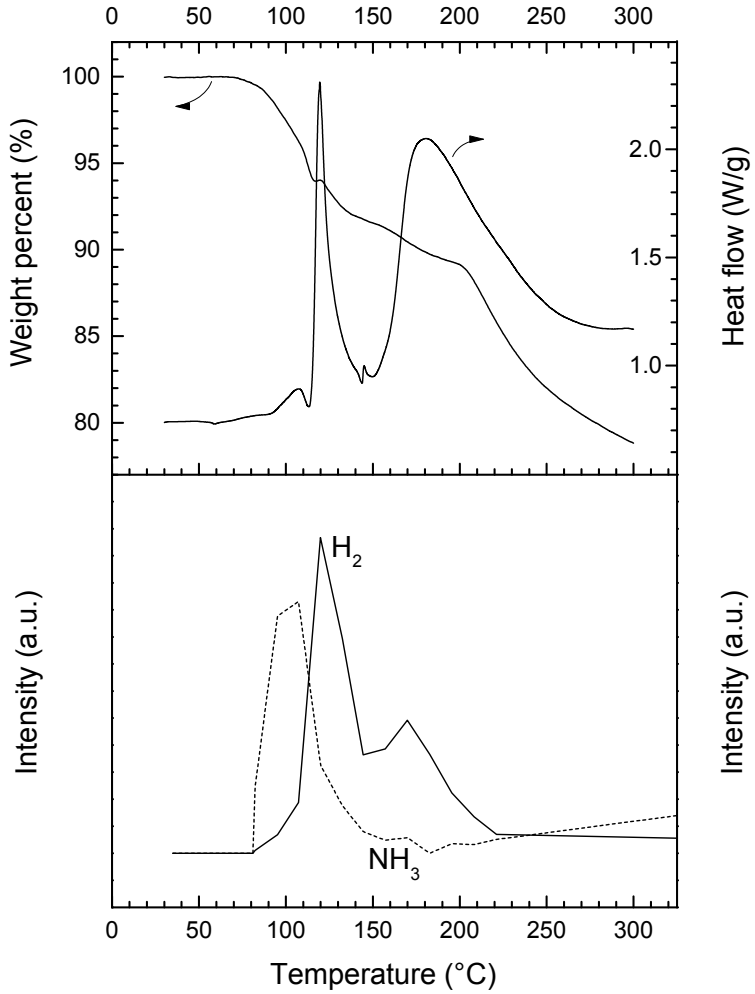

Figure 4. TGA, DSC, and μGC-MS (H_2 $m/z = 2$, NH_3 $m/z = 17$) data for **3** (heating rate of 5 °C min^{-1}).

In our conditions, **3** releases most of the NH_3 during the first decomposition step. Similar trends were reported for lithium amidoborane ammoniate $Li(NH_2BH_3) \cdot NH_3$, for which the evolution of NH_3 peaks at 52 °C while that of H_2 shows the maximum at around 100 °C [23]. Similar observations were reported for calcium amidoborane ammoniate $Ca(NH_2BH_3) \cdot NH_3$, making the authors suggest that the adducted NH_3 is weakly bound to the cation Ca^{2+} [13].

In our laboratory, TGA has been used as an efficient screening tool to evaluate the potential of any new B–N–H compound as well as to compare several of them. Accordingly, the thermal behavior of the sample **3** was first compared to that of the reactants **1** and **2**. The TGA curves are shown

in Figure 5. In comparison, **2** is quite stable under heating at 5 °C min^{-1}. The weight loss of about 0.6 wt% is negligible before 200 °C and increases to 2.5 wt% up to 300 °C. With respect to **1**, it has a much different TGA profile. Therefore, **3** is a compound that is different from the precursors. As mentioned in the previous paragraphs, **3** is somehow comparable to the ammonia-free derivative $LiN_2H_3BH_3$ (denoted **4** in Figure 5). So, the thermal behavior of **3** was also compared to that of **4**. It is worth mentioning that **4** is known to dehydrogenate according to a complex mechanism not releasing unwanted by-products like NH_3 [7,8]. The thermal behaviors of these two compounds are different. **3** starts its decomposition at a lower temperature than **4** and shows a higher weight loss due to the release of NH_3 molecules from both the complexation and the decomposition phenomena. In other words, the presence of NH_3 in **3** leads to a thermolytic behavior which is different from that observed with **4**.

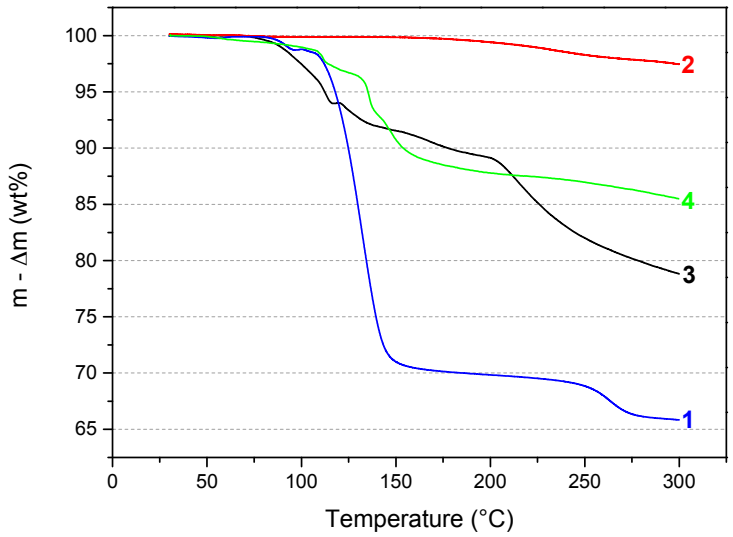

Figure 5. Superimposition of the TGA curves of **1** ($N_2H_4BH_3$; from ref. [5]), **2** ($LiNH_2$), **3** ($LiN_2H_3BH_3{\cdot}xNH_3$), and **4** ($LiN_2H_3BH_3$; from ref. [8]).

3. Discussion and Concluding Remarks

In good agreement with our primary objective, a new hydrogen-rich B–N–H compound has been successfully synthesized by solid-state reaction (mechanosynthesis/ball-milling) of $N_2H_4BH_3$ and $LiNH_2$. The molecular analyses suggest a compound with the formula $LiN_2H_3BH_3{\cdot}xNH_3$. This is a new type of coordination compound consisting of a metal cation Li^+, a $[N_2H_3BH_3]^-$ anionic unit, and an xNH_3 ligand [24]. The crystallographic analysis allowed quantifying the x value thanks to the difference in the cell volumes of $LiN_2H_3BH_3{\cdot}xNH_3$ and another well-described derivative—$LiN_2H_3BH_3$. Indeed, x was found to be equal to 0.25 suggesting then the following reaction:

$$LiNH_2\ (s) + N_2H_4BH_3\ (s) \rightarrow LiN_2H_3BH_3{\cdot}0.25NH_3\ (s) + 0.75NH_3\ (g) \quad (3)$$

Note that we also worked on a mixture of $LiNH_2$ and $N_2H_4BH_3$ (results not reported) where the mole ratio was lower than 1. We indeed considered 0.75 mole of $LiNH_2$ and 1 mole of $N_2H_4BH_3$. Like for $LiN_2H_3BH_3{\cdot}0.25NH_3$, a paste-like solid was obtained. The as-obtained product showed NMR and FTIR spectra that were comparable to those of $LiN_2H_3BH_3{\cdot}0.25NH_3$. With respect to the powder XRD pattern, the diffraction peaks were comparable to those observed for $LiN_2H_3BH_3{\cdot}0.25NH_3$, but with additional peaks belonging to the excess of $N_2H_4BH_3$. The TGA results were also comparable. In other words, the results and the observations were consistent with the occurrence of the reaction shown by Equation (3).

The reaction of $LiNH_2$ and $N_2H_4BH_3$ in our conditions can be interpreted as follows. The Lewis base NH_2 of $LiNH_2$ would favorably react with the acidic hydrogen $H^{\delta+}$ of the N_2H_4 moiety of the borane resulting in NH_3. In parallel, the Li^+ cation would combine with the $H^{\delta+}$-deficient $N_2H_3^-$ entity towards the formation of the entity $LiN_2H_3BH_3$. It seems that a quarter of the as-formed NH_3 complexes $LiN_2H_3BH_3$ leading to the formation of a $LiN_2H_3BH_3{\cdot}0.25NH_3$ like-compound. The rest of the NH_3 (the 0.75 equivalent) can be evacuated under vacuum at ambient conditions.

Ammonia is known to have good affinity with the B–N–H compounds. A first example is ammonia borane. Exposed to an atmosphere of NH_3, NH_3BH_3 is able to complex up to six molecules of NH_3, resulting in the formation of a pasty solid [25]. Furthermore, NH_3 is an excellent solvent of NH_3BH_3; the solubility is 259.7 g of NH_3BH_3 in 100 g of NH_3 and the solvated borane shows good stability [26]. A second example is an alkali derivative of NH_3BH_3. It was observed that exposure of $LiNH_2BH_3$ to NH_3 produces a sticky liquid containing a 1:1 molar ratio of $LiNH_2BH_3$ to NH_3 [23]. Keeping in mind these reported observations, we did a simple experiment. We synthesized $LiN_2H_4BH_3$ as reported in our previous report [8] and exposed it to a stream of NH_3. Like for the aforementioned $LiNH_2BH_3$ [23], our sample changed to a sticky liquid/pasty material. Hence, we may conclude that the "excess" of 0.75 mole of NH_3 (Equation (3)) explains the paste-like state of **3** right after ball-milling.

The new compound $LiN_2H_3BH_3{\cdot}0.25NH_3$ was primarily synthesized for assessing its potential as chemical H storage material. Ammoniates of B–N–H compounds are of interest as, compared to their ammonia-free counterparts, they should have better dehydrogenation properties owing to the active participation of NH_3 in the dehydrogenation process [13]. In our conditions, $LiN_2H_3BH_3{\cdot}xNH_3$ has been shown to release H_2 at temperatures lower than $LiN_2H_3BH_3$, which is consistent with the previous remark. However, $LiN_2H_3BH_3{\cdot}0.25NH_3$ liberates non-negligible amounts of NH_3. According to Chua et al. [13], contamination of H_2 by small amounts of NH_3 is unavoidable, but in our conditions the amount of NH_3 represents 7.6 wt% of the starting material. Under heating, the x molecules of NH_3 are first released at temperatures lower than 100°C, and then the remaining solid, supposed to be mainly $LiN_2H_3BH_3$, decomposes into H_2 and NH_3. Taking into account the overall weight loss of 21.2 wt% between 75 and 300 °C and the contents of H (12.1 wt%) and NH_3 (7.6 wt%) in $LiN_2H_3BH_3{\cdot}0.25NH_3$, there is a difference of 1.5 wt% (assuming the loss of all H atoms). This is indicative of the decomposition of $LiN_2H_3BH_3{\cdot}0.25NH_3$ to some extent. For example, if one assumes the formation of 2 equivalents of H_2 up to 300 °C (i.e., 7.7 wt%, which means the loss of 4 H atoms over a maximum of 6 in $LiN_2H_3BH_3$), the proportion of NH_3 stemming from the decomposition of $LiN_2H_3BH_3$ would be 5.9 wt% at 300 °C. This is illustrated in Figure 6 where a mechanism of decomposition is suggested on the basis of both the present results and the results reported for $LiN_2H_3BH_3$ elsewhere [8]. A polymeric product of unknown composition forms, similar to the residues recovered upon the dehydrogenation of most of the B–N–H compounds [5–12,27]. The nature of such residues is unknown yet because of their difficult characterization (amorphous to X-ray and too complex composition for FTIR and NMR spectroscopy techniques).

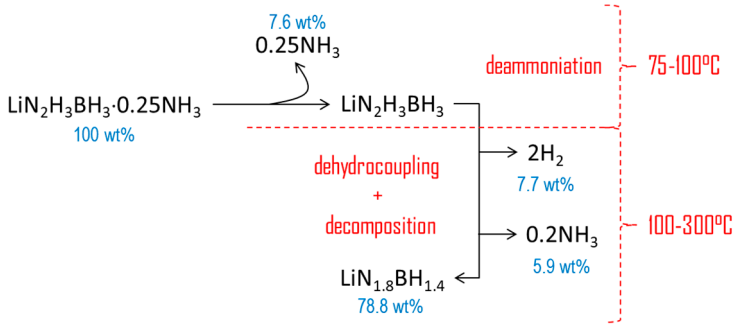

Figure 6. TGA results-based proposition of a decomposition mechanism of $LiN_2H_3BH_3{\cdot}0.25NH_3$.

With respect to the aforementioned release of NH_3, such a feature is unfortunately quite detrimental for the targeted application, namely chemical H storage. Indeed, the stored hydrogen is intended to be generated on demand for fueling a low-temperature fuel cell, but traces of ammonia (as low as 1 ppm) are able to severely degrade the fuel cell performance to impractical levels [28]. Given that the release of the 0.25 NH_3 cannot be avoided with $LiN_2H_3BH_3{\cdot}0.25NH_3$, its ammonia-free counterpart $LiN_2H_3BH_3$ [8] seems to be more suitable for chemical H storage.

Yet, our new compound $LiN_2H_3BH_3{\cdot}0.25NH_3$ might have potential for another application. It might be seen as a potential NH_3 carrier as it is theoretically able to release 7.6 wt% of NH_3 from 75 °C.

4. Materials and Methods

Hydrogen-storage grade $LiNH_2$ was purchased from Sigma-Aldrich and used as received. Hydrazine borane $N_2H_4BH_3$ was synthesized by salt metathesis according to an optimized procedure reported in details elsewhere [5]. Typically, an equimolar mixture of sodium borohydride $NaBH_4$ (Acros Organics, Geel, Belgium) and hydrazine hemisulfate $N_2H_4{\cdot}1/2H_2SO_4$ (Sigma-Aldrich, St Quentin Fallavier, France) in dioxane were prepared in a 250-mL three-necked round-bottom flask kept under argon flow. The mixture was allowed to react at 40 °C for 48 h. Then, the solution of $N_2H_4BH_3$ was separated from insoluble Na_2SO_4 by filtration, the solvent was removed by extraction under vacuum at room temperature for 4 h, and the as-obtained borane was dried under dynamic vacuum at room temperature for 24 h. Both $LiNH_2$ and $N_2H_4BH_3$ were stored and handled in an argon-filled glove box (MBraun M200B, O_2 < 0.1 ppm, H_2O < 0.1 ppm).

The synthesis of our new compound was done as follows. In the argon-filled glove box, $LiNH_2$ and $N_2H_4BH_3$ were separately weighted (total of about 350 mg; equimolar ratio) and transferred in a 50-mL stainless steel jar. Several stainless steel balls (Ø 10 mm) of a total weight of 40 g were added and the jar was sealed to be taken out of the glove box. The mixture was ball-milled at ambient conditions by using a RETSCH PM 100 planetary ball mill: 2 min of milling at 300 rpm + 2 min of break, 10 times. In doing so, a paste-like solid was obtained. It was subjected to vacuum overnight. The paste-like state was modified, appearing less pasty. The sample was finally transferred into a vial to be kept in the argon-filled glove box. Note that these conditions were optimized in a preliminary systematic study (not reported herein). We indeed worked with different $N_2H_4BH_3/LiNH_2$ ratios (1:0.75 and 1:0.5), using different ball-milling conditions and a wet synthesis approach (solubilization/dispersion of the reactants in moisture-free organic solvents like tetrahydrofuran and dioxane). For consistency and clarity, only the optimized conditions are presented.

The molecular structure was analyzed by Fourier transform infrared (FTIR) spectroscopy (Nicolet 710, range 3600–600 cm^{-1}, 32 scans). The attenuated total reflection (ATR) mode (enabling sample to be examined directly) was used at ambient conditions and under air. To minimize the contact of the sample with atmospheric O_2 and H_2O, a vial containing a few milligrams of the borane was prepared in the glove box, taken out, and opened just before the measurement. The number of scans was fixed to 32 to avoid excessive contact with air. In such conditions, reliable spectra are generally collected.

The molecular structure was also analyzed by ^{11}B magic-angle spinning nuclear magnetic resonance (MAS NMR) spectroscopy (Varian VNMR400, 128.37 MHz, 20000 rpm, −10 °C). In the glove box, a few milligrams (or grains) of the sample was transferred into the NMR tube (Ø 10 mm) and dissolved by acetonitrile-d3 (Eurisotop, Gif sur Yvette, France). The sealed tube was then taken out of the glove box to be analyzed by NMR according to the standard procedures for this technique.

The crystal structure was analyzed by powder X-ray diffraction (PXRD) using a PANalytical X'PERT Pro multipurpose diffractometer (Cu-$K_{\alpha 1/\alpha 2}$ radiation, λ = 1.5418 Å, 45 kV, 30 mA). All the patterns were collected using Bragg–Brentano geometry on a spinning sample holder loaded into a glove box (Jacomex PBOX, H_2O < 5 ppm, O_2 < 5 ppm). The powders were protected from air and oxygen contamination using a Kapton foil.

The thermal behavior of the samples was analyzed by thermogravimetric analysis (TGA; Q500 TA Instruments; heating rate 5 °C min^{-1}; N_2 flow rate 50 mL min^{-1}) and differential scanning calorimetry (DSC; 2920 MDSC TA Instruments, manufacturer, New Castle, DE, USA). For both techniques, our standard conditions were as follows: sample weight of 2–3 mg; aluminum crucible of 100 mL with a pinhole (Ø 670 mm); temperature range 25–300 °C; heating rate 5 °C min^{-1}; N_2 flow rate of 50 mL min^{-1}. A micro-gas chromatograph-mass spectrometer detector (μGC-MSD; S.R.A. Instruments, Agilent Technologies, Lyon, France) was used in coupling with a TGA/DSC 2 from Mettler-Toledo for the identification and quantification of the gaseous by-products. The μGC is equipped with micro-thermal conductivity detectors and two columns: one molecular sieve column for the detection and quantification of H_2 (10 m × 0.32 mm; 5 Å; carrier gas Ar; 70 °C; head column pressure fixed at 28 psi), and one poraPLOT U column for NH_3 (8 m × 0.15 mm i.d.; carrier gas He; 130°C; head column pressure fixed at 30 psi).

Acknowledgments: This work has been partially funded by the French State via the ANR (Agence Nationale de la Recherche) and the program "Investissements d'Avenir" with the reference ANR-10-LABX-05-01. The work has also been partially funded by the Région Languedoc-Roussillon and the program "Chercheur(se)s d'Avenir 2013" (project C3/2013 008555). U.B.D. thanks Jean-Fabien Petit for a few of the preliminary ball-milling syntheses, Torben R. Jensen (Aarhus University) for suggesting the use of $LiNH_2$, and Lars Jepsen (Aarhus University) for his help in XRD.

Author Contributions: S.O.A. did most of the experimental work within the frame of his PhD thesis. D.G. did the XRD analyses. R.C. and F.T. were in charge with the thermal characterizations as well as the evolved gas analyses. P.G.Y. was in charge with the crystal structure determination and the treatment of XRD data; he is the co-supervisor of S.O.A. U.B.D. is the leader of the project and the main supervisor of S.O.A.; he also analyzed the molecular data and wrote most of the paper.

Conflicts of Interest: The authors declare no conflict of interest.

References

1. Sherif, S.A.; Goswami, D.Y.; Stefanakos, E.K.; Steinfeld, A. *Handbook of Hydrogen Energy*; CRC Press: New York, NY, USA, 2014.
2. Staubitz, A.; Robertson, A.P.M.; Sloan, M.E.; Manners, I. Amine- and phosphine-borane adducts: New interest in old molecules. *Chem. Rev.* **2010**, *110*, 4023–4078. [CrossRef] [PubMed]
3. Goubeau, V.J.; Ricker, E. Borinhydrazin und seine pyrolyseprodukte. *Z. Anorg. Allg. Chem.* **1961**, *310*, 123–142. [CrossRef]
4. Hügle, T.; Kühnel, M.F.; Lentz, D. Hydrazine borane: A promising hydrogen storage material. *J. Am. Chem. Soc.* **2009**, *131*, 7444–7446. [CrossRef] [PubMed]
5. Moury, R.; Moussa, G.; Demirci, U.B.; Hannauer, J.; Bernard, S.; Petit, E.; van der Lee, A.; Miele, P. Hydrazine borane: Synthesis, characterization, and application prospects in chemical hydrogen storage. *Phys. Chem. Chem. Phys.* **2012**, *14*, 1768–1777. [CrossRef] [PubMed]
6. Moury, R.; Demirci, U.B. Hydrazine borane and hydrazinidoboranes as chemical hydrogen storage materials. *Energies* **2015**, *8*, 3118–3141. [CrossRef]
7. Wu, H.; Zhou, W.; Pinkerton, F.E.; Udovic, T.J.; Yildirim, T.; Rush, J.J. Metal hydrazinoborane $LiN_2H_3BH_3$ and $LiN_2H_3BH_3{\cdot}2N_2H_4BH_3$: Crystal structures and high-extent dehydrogenation. *Energy Environ. Sci.* **2012**, *5*, 7531–7535. [CrossRef]
8. Moury, R.; Demirci, U.B.; Ban, V.; Filinchuk, Y.; Ichikawa, T.; Zeng, L.; Goshome, K.; Miele, P. Lithium hydrazinidoborane, a polymorphic material with potential for chemical hydrogen storage. *ChemSusChem* **2014**, *26*, 3249–3255. [CrossRef]
9. Moury, R.; Demirci, U.B.; Ichikawa, T.; Filinchuk, Y.; Chiriac, R.; van der Lee, A.; Miele, P. Sodium hydrazinidoborane, a chemical hydrogen storage material. *ChemSusChem* **2013**, *6*, 667–673. [CrossRef] [PubMed]
10. Pylypko, S.; Petit, J.F.; Ould-Amara, S.; Ndhili, N.; Taihei, A.; Chiriac, R.; Ichikawa, T.; Cretin, M.; Miele, P.; Demirci, U.B. Metal hydride-hydrazine borane: Towards hydrazinidoboranes or composites as hydrogen carriers. *Int. J. Hydrogen Energy* **2015**, *40*, 14875–14884. [CrossRef]

11. Chua, Y.S.; Pei, Q.; Ju, X.; Zhou, W.; Udovic, T.J.; Wu, G.; Xiong, Z.; Chen, P.; Wu, H. Alkali metal hydride modification on hydrazine borane for improved dehydrogenation. *J. Phys. Chem. C* **2014**, *118*, 11244–11251. [CrossRef]
12. Chua, Y.S.; Wu, G.; Xiong, Z.; Karkamkar, A.; Guo, J.; Jian, M.; Wong, M.W.; Autrey, T.; Chen, P. Synthesis, structure and dehydrogenation of magnesium amidoborane monoammoniate. *Chem. Commun.* **2010**, *46*, 5752–5754. [CrossRef] [PubMed]
13. Chua, Y.S.; Wu, G.; Zhou, W.; Udovic, T.J.; Wu, G.; Xiong, Z.; Wong, M.W.; Chen, P. Monoammoniate of calcium amidoborane: Synthesis, structure, and hydrogen-storage properties. *Inorg. Chem.* **2012**, *51*, 1599–1603. [CrossRef] [PubMed]
14. Yan, Y.; Remhof, A.; Rentsch, D.; Züttel, A.; Giri, S.; Jena, P. A novel strategy for reversible hydrogen storage in $Ca(BH_4)_2$. *Chem. Commun.* **2015**, *51*, 11008–11011. [CrossRef] [PubMed]
15. Esteruelas, M.A.; Nolis, P.; Oliván, M.; Oñate, E.; Vallribera, A.; Vélez, A. Ammonia borane dehydrogenation promoted by a pincer-square-planar rhodium(I) monohydride: A stepwise hydrogen transfer from the substrate to the catalyst. *Inorg. Chem.* **2016**, *55*, 7176–7181. [CrossRef] [PubMed]
16. Stowe, A.C.; Shaw, W.J.; Linehan, J.C.; Schmid, B.; Autrey, T. In situ solid state ^{11}B MAS-NMR studies of the thermal decomposition of ammonia borane: Mechanistic studies of the hydrogen release pathways from a solid state hydrogen storage material. *Phys. Chem. Chem. Phys.* **2007**, *9*, 1831–1836. [CrossRef] [PubMed]
17. Wu, H.; Zhou, W.; Pinkerton, F.E.; Meyer, M.S.; Srinivas, G.; Yildirim, T.; Udovic, T.J.; Rush, J.J. A new family of metal borohydride ammonia borane complexes: Synthesis, structures, and hydrogen storage properties. *J. Mater. Chem.* **2010**, *20*, 6550–6556. [CrossRef]
18. Yot, P.G.; Miele, P.; Demirci, U.B. In situ Synchrotron X-ray thermodiffraction of boranes. *Crystals* **2016**, *6*, 16. [CrossRef]
19. Yang, J.B.; Zhou, X.D. Crystal and electronic structures of $LiNH_2$. *Appl. Phys. Lett.* **2006**, *88*, 041914. [CrossRef]
20. Boultif, A.; Louer, D. Indexing of powder diffraction patterns for low-symmetry lattices by the successive dichotomy method. *J. Appl. Crystallogr.* **1991**, *24*, 987–993. [CrossRef]
21. Altomare, A.; Cuocci, C.; Giacovazzo, C.; Moliterni, A.; Rizzi, R.; Corriero, N.; Falcicchio, A. EXPO2013: A kit of tools for phasing crystal structures from powder data. *J. Appl. Crystallogr.* **2013**, *46*, 1231–1235. [CrossRef]
22. Petricek, V.; Dusek, M.; Palatinus, L. Crystallographic Computing System JANA2006: General features. *Z. Kristallogr.* **2014**, *229*, 345–352. [CrossRef]
23. Xia, G.; Yu, X.; Guo, Y.; Wu, Z.; Yang, C.; Liu, H.; Dou, S. Amminelithium amidoborane $Li(NH_3)NH_2BH_3$: A new coordination compound with favorable dehydrogenation characteristics. *Chem. Eur. J.* **2010**, *16*, 3763–3769. [CrossRef] [PubMed]
24. Kang, X.; Wu, H.; Zhou, W.; Wang, P. A simple and efficient approach to synthesize amidoborane ammoniates: Case study for $Mg(NH_2BH_3)_2(NH_3)_3$ with unusual coordination structure. *J. Mater. Chem.* **2012**, *22*, 13174–13179. [CrossRef]
25. Gao, L.; Fang, H.; Li, Z.; Yu, X.; Fan, K. Liquefaction of solid-state BH_3NH_3 by gaseous NH_3. *Inorg. Chem.* **2011**, *50*, 4301–4306. [CrossRef] [PubMed]
26. Shore, S.G.; Parry, R.W. The crystalline compound ammonia-borane, H_3NBH_3. *J. Am. Chem. Soc.* **1955**, *77*, 6084–6085. [CrossRef]
27. Summerscales, O.T.; Gordon, J.C. Regeneration of ammonia borane from spent fuel materials. *Dalton Trans.* **2013**, *42*, 10075–10084. [CrossRef] [PubMed]
28. Halseid, R.; Vie, P.J.S.; Tunold, R. Effect of ammonia on the performance of polymer electrolyte membrane fuel cells. *J. Power Sources* **2006**, *154*, 343–350. [CrossRef]